THE JOURNAL OF PHYSICAL CHEMISTRY B
A JOURNAL OF THE AMERICAN CHEMICAL SOCIETY

pubs.acs.org/JPCB

Article

Effect of Ion Mass on Dynamic Correlations in Ionic Liquids

Md. Dipu Ahmed, Zhenghao Zhu, Airat Khamzin, Stephen J. Paddison, Alexei P. Sokolov, and Ivan Popov*

Cite This: *J. Phys. Chem. B* 2023, 127, 10411−10421

Read Online

ACCESS | Metrics & More | Article Recommendations | Supporting Information

ABSTRACT: Ionic liquids (ILs) are a class of liquid salts with distinct properties such as high ionic conductivity, low volatility, and a broad electrochemical window, making them appealing for use in energy storage applications. The ion−ion correlations are some of the key factors that play a critical role in the ionic conductivity of ILs. In this work, we present the study of the impact of ion mass on ion−ion correlations in ILs, applying a combination of broadband dielectric spectroscopy measurements and molecular dynamics simulations. We examined three ILs with the same cation but different anions to consider three different cases of cation−anion masses: $M_+ > M_-$, $M_+ \approx M_-$, and $M_+ < M_-$. We applied the momentum conservation approach to estimate the contribution of distinct ion−ion correlations from experimental data and obtained good agreement with direct calculations of distinct ion−ion correlations from molecular dynamics simulations. Our findings reveal that relative ion mass has a strong effect on the distinct ion−ion correlations, leading to swapping of the relative amplitude of distinct cation−cation and anion−anion correlations.

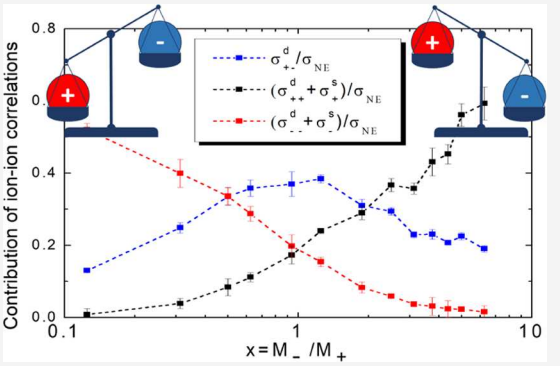

INTRODUCTION

Room-temperature ionic liquids (ILs) are promising materials for various electrochemical energy storage applications, including batteries and supercapacitors.[1−3] ILs demonstrate high intrinsic conductivity, low flammability, and higher thermal and electrochemical stabilities in comparison to conventional salt solutions with carbonate solvents.[4−7] Due to these characteristics, they meet most of the criteria for electrochemical devices with improved performance and safety.[8] One of the key fundamental properties of any ionic system is its ionic conductivity. In diluted salt solutions, ionic conductivity can be estimated using the Nernst−Einstein (NE) equation from information concerning the concentration, n_i, and self-diffusion coefficient, D_i^s, of the mobile ions[9,10]

$$\sigma_{NE} = \frac{q^2}{k_B T} \sum_i n_i D_i^s \tag{1}$$

where q is the charge of an ion. In diluted salt solutions, where ion−ion interactions are assumed to be negligible, the experimentally measured ionic conductivity (σ_{DC}) indeed is very close to the estimation from eq 1 ($\sigma_{DC} \approx \sigma_{NE}$). However, concentrated ionic systems, including ILs, have significant ion−ion interactions, leading to strong dynamic correlations of ions. As a result, the NE equation fails to describe the ionic conductivity of concentrated systems,[9−19] and the additional factor has to be introduced to the NE equation[9,20,21]

$$\sigma_{DC} = H^{-1}\sigma_{NE} = H^{-1}\frac{q^2}{k_B T} \sum_i n_i D_i^s \tag{2}$$

Here, the ratio $H^{-1} = \sigma_{DC}/\sigma_{NE}$ is known as ionicity or inverse Haven ratio.[13,22] The ionicity of ILs is always less than one (i.e., $H^{-1} < 1$),[13,15,16,23−26] and this has been traditionally ascribed to the presence of ion pairs due to the coupled motion of anion and cation.[1,27] However, recent simulations[28] and experiments[29−31] have revealed that the low value of H^{-1} for molten salts and ionic liquids is mostly caused by distinct anion−anion and cation−cation correlations, rather than the ion pairs. Even more interesting effects occur in the mixtures of salt and ionic liquids, where ion−ion correlations lead to clustering and surprising negative cation transport numbers,[32−35] or even superionic behavior[36] with $H^{-1} > 1$.

Molecular dynamics (MD) simulations have been the only method for estimating the contribution of distinct ion−ion correlations to conductivity. Recently, a method was proposed from experimental measurements.[37] However, the proposed approach is complex and challenging, requiring electrodes containing one ion (e.g., Li^+), and has been applied only to a

Received: August 17, 2023
Revised: November 13, 2023
Accepted: November 14, 2023
Published: November 27, 2023

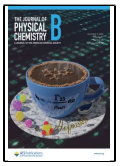

https://doi.org/10.1021/acs.jpcb.3c05568
J. Phys. Chem. B 2023, 127, 10411−10421

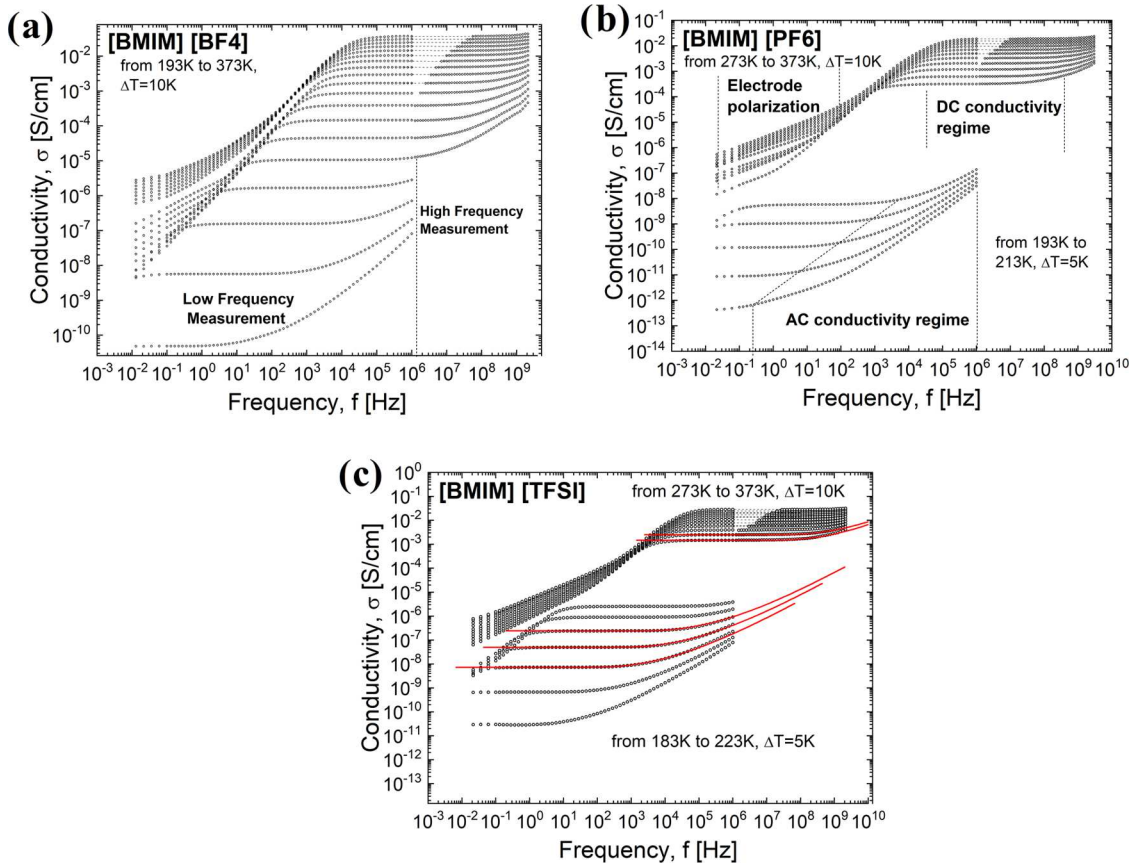

Figure 1. Conductivity spectra over a wide frequency range for the different ionic liquids: (a) [BMIM][BF4]; (b) [BMIM][PF6]; and (c) [BMIM][TFSI]. In panel (b), the different regimes are shown: (1) AC conductivity; (2) DC conductivity; and (3) electrode polarization. To determine the conductivity relaxation time, τ_σ, the conductivity spectra were fitted using eq 7. The example of fitting at different temperatures is shown in panel (c) by red solid lines. To match data from high- and low-frequency measurements, the electrode polarization regime in the high-frequency measurements was removed, and dashed lines are displayed only to guide the eye.

few lithium conductive systems. Another approach that was proposed in refs. 38,39 is based on a combination of experimental measurements of conductivity and diffusion and theoretical models and the assumption that the total momentum of all ions is conserved. Recently, this approach was used to estimate each term of the distinct ion−ion correlations in polymerized ionic liquids,[39] ionic liquids,[28,30] and concentrated solutions.[40] However, the estimations of the distinct ion−ion correlations from experimental data using this approach were never compared to the results of model-independent MD investigations.

To verify the validity of the momentum conservation approach, we performed experimental and computational studies of ILs with different ion masses. We chose ILs with the same cation, 1-butyl-3-methylimidazolium ([BMIM], M_+ ≈139 g/mol), but different anions, [BF_4] (M_- ≈ 87 g/mol), [PF_6] (M_- ≈145 g/mol), and bis(trifluoromethane)-sulfonimide [TFSI](M_- ≈280 g/mol). These ILs present the cases when $M_- < M_+$ [BMIM]-[BF4], $M_- \approx M_+$ [BMIM]-[PF6], and when $M_- > M_+$ [BMIM]-[TFSI]. Experimental data were used to estimate distinct ionic correlations based on the momentum conservation approach, and the results were compared to MD simulations, where distinct ion−ion correlations were directly computed. This comparison revealed a good quantitative agreement between experimental and simulation results. In particular, the cation−cation correlations provide a more negative contribution to conductivity than the anion−anion correlations in [BMIM]-[BF]4 with $M_- < M_+$, while in [BMIM]-[TFSI] with $M_- > M_+$, the anion−anion correlations contribute more negatively to conductivity than the cation−cation correlations. At the same time, the cation−anion correlation has a positive contribution to conductivity in all three ILs. We also discuss how the momentum conservation approach depends on the choice of coordinate system.

EXPERIMENTAL RESULTS

Materials. 1-Butyl-3-methylimidazolium tetrafluoroborate [BMIM][BF4], 1-butyl-3-methylimidazolium hexafluorophosphate [BMIM][PF6], and 1-butyl-3-methylimidazolium bis(trifluoromethylsulfonyl)imide [BMIM][TFSI] were purchased from Sigma-Aldrich and used as purchased. The samples were opened and loaded into a cell for conductivity measurements inside a glovebox in an inert atmosphere.

Broadband Dielectric Spectroscopy (BDS). BDS was used to perform conductivity spectra measurements. Two spectrometers were utilized to cover the wide frequency range from 0.1 Hz up to 3 GHz. An α-A analyzer from Novocontrol was utilized in the frequency range of 10^{-1}−10^6 Hz. A cell consists of a cap as the bottom electrode; the upper electrode is separated from the cap by a sapphire window to avoid electrical contact between them. The fixed electrode distance of 0.4 mm and a diameter of 10.2 mm were used. The samples were measured with a voltage amplitude of 0.1 V. The standard calibration procedure was used before measurements. An

https://doi.org/10.1021/acs.jpcb.3c05568
J. Phys. Chem. B 2023, 127, 10411−10421

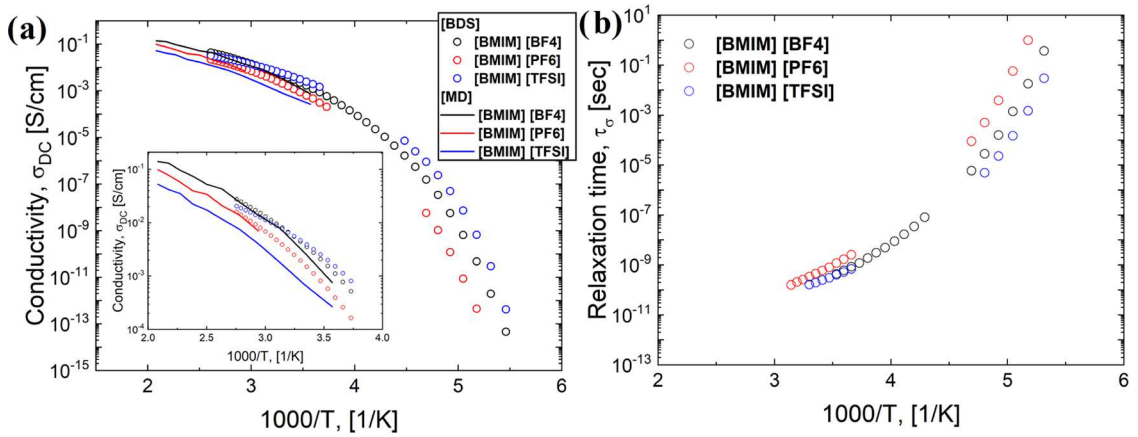

Figure 2. (a) Temperature dependence of the DC conductivity, σ_{DC}: symbols present experimental data, and lines are from the MD simulations results. The inset figure in panel (a) represents the comparison of MD results and experimental data on an expanded scale. (b) Temperature dependence of the conductivity relaxation time, τ_σ. The gap in the experimental data for σ_{DC} and τ_σ at low temperatures for [BMIM][PF6] and [BMIM][TFSI] is due to crystallization.

Agilent RF impedance material analyzer, E4991A, with WinDETA Software from Novocontrol, was used in the frequency range 10^6−3 × 10^9 Hz. The cell was constructed using two APC-7 connectors. For the upper electrode, the inner pin of one connector was replaced by a solid pin with a diameter of 3 mm, and the free space between the inner pin and outer part was filled by Teflon. For the lower electrode, the pin in the other connector was removed, and in the free central space, a movable metallic cylinder was inserted. As a result, the coaxial line was terminated by a plate capacitor with an adjustable distance between the electrodes. The coaxial line was calibrated using a standard procedure (Open/Short/50 Ω) to move the reference plane up to the cell terminating the line. The cell was also calibrated (open and short) for better precision. The samples were loaded between the two electrodes at 0.1 mm and measured with a voltage amplitude of 0.1 V. A Quattro temperature controller (Novocontrol) was used for temperature stabilization for the measurements from 10^{-1} to 10^9 Hz. The samples were stabilized for 20 min at each temperature to reach a precision of ±0.2 K. The samples were equilibrated at each temperature for 20 min to achieve a precision of ±0.2 K, followed by rapid quenching to prevent crystallization at low temperatures and to reach supercooled liquid states. However, the two ionic liquids [BMIM][PF6] and [BMIM][TFSI] crystallized upon heating and then melted back at higher temperatures. In our further analysis, the conductivity data corresponding to the crystalline states of the ILs were excluded.

The conductivity spectra for all studied systems exhibit three usual regions (Figure 1a−1c): (i) frequency-dependent AC conductivity regime at high frequencies, σ_{AC}; (ii) a plateau level of DC conductivity regime at the intermediate frequency range, σ_{DC}, and (iii) a decrease due to the accumulation of charge carriers at the surface of the electrode at a lower frequency (electrode polarization effect).[41] The temperature gap in the data for [BMIM][PF6] and [BMIM][TFSI] is caused by sample crystallization.

Molecular Dynamic (MD) Simulations. MD simulations were performed for a variety of molecular BMIM-based ILs. Each system consisted of 500 pairs of ions, providing an optimal balance between statistical reliability and computational efficiency.[42−44] The methodology was established by using the generalized AMBER force field (GAFF) utilizing a previously employed protocol.[45−48] Partial charges on all atoms were determined with the restrained electrostatic potential (RESP) algorithm[49] based on the optimized electronic structures of the isolated cation or anion. These *ab initio* calculations were carried out at the Hartree−Fock HF/6−31g(d) level of theory using the Gaussian 09 package.[50] The computed atomic partial charges were scaled by a factor of 0.8 to account for polarization and charge transfer, which has been proven to be an efficient and reliable approach in ion-containing systems.[48,51,52] A cutoff distance of 14 Å was used for the electrostatic and Lennard-Jones interactions with long-range corrections handled by the particle mesh Ewald (PME) method and appropriate tail corrections, respectively. The initial systems were equilibrated for over 50 ns within the NPT ensemble, following a ∼ 30 ns annealing process using the GROMACS code.[53] Following an additional 30 ns of equilibration under the NVT ensemble, a trajectory of 100 ns was collected every 1 ps. This length of trajectory ensured reliable ion−ion correlations in these IL systems.[12,54] Temperature and pressure were controlled by the Bussi thermostat[55] and the Parrinello-Rahman barostat[56] with coupling times of 0.5 and 5 ps, respectively. The MD simulations for all of the IL systems were conducted in a periodic cubic box with a time step of 2 fs. To assess the accuracy of the force fields applied to these systems, we compared the simulation and experimental densities, as illustrated in Figure S1. The density of [BMIM][TFSI] closely matches the experimental data. While the densities of the other two systems are slightly lower than the experimental values,[23] they still exhibit reasonable agreement. All dynamic correlations were compiled from 4 to 6 trajectories to provide average values, along with their corresponding standard deviations.

DISCUSSION

The conductivity spectra of ion conductive materials[10,11] are usually described by the random barrier model (RBM).[57−60] According to this model, charge carriers hop over potential energy barriers. When the barrier height distribution is constant, the model results in the following equation[61]

$$\ln\left(\frac{\sigma^*(\omega)}{\sigma_{DC}}\right) = \frac{i\omega\tau_\sigma\sigma_{DC}}{\sigma^*(\omega)}\left(1 + \frac{8}{3}\frac{i\omega\tau_\sigma\sigma_{DC}}{\sigma^*(\omega)}\right)^{-1/3} \quad (3)$$

https://doi.org/10.1021/acs.jpcb.3c05568
J. Phys. Chem. B 2023, 127, 10411−10421

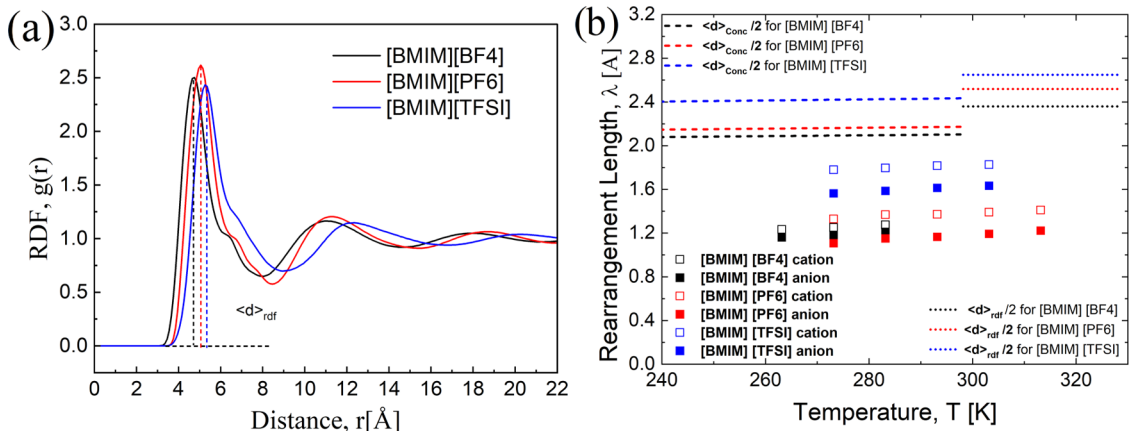

Figure 3. (a) Radial distribution functions of the center of mass of cations and anions in ILs to estimate half the average distance between the ions, $\langle d \rangle_{rdf}/2$. (b) Ions rearrangement length estimated from eq 8 for cations (open square symbols) and anions (closed square symbols). Estimated half distances between the ions from ion concentration, $\langle d \rangle_{conc}/2$, are represented by dashed lines. Estimated half distances between the ions from the radial distribution functions, $\langle d \rangle_{rdf}/2$, are represented by dotted lines.

Here, $\sigma^*(\omega)$ is a measured complex conductivity, σ_{DC} is a DC conductivity, and τ_σ is a conductivity relaxation time. The latter specifies the characteristic of AC−DC crossover time when charge mean-squared displacement crosses over from a subdiffusive regime, $\langle r^2(t) \rangle \sim t^\alpha$ with $\alpha < 1$ (corresponds to AC tail in conductivity spectra) to a normal diffusion regime $\langle r^2(t) \rangle \sim t$ (corresponds to DC-plateau in conductivity spectra). Both the conductivity spectra and the conductivity relaxation process in the real part of the dielectric permittivity are described by eq 3. The examples of conductivity spectra fits are shown in Figure 1c, and the temperature dependences of σ_{DC} and τ_σ obtained from the fits are plotted in Figure 2. The results for conductivity values from MD simulations are presented in the same Figure 2a and provide a good match with experimentally measured data for [BMIM][BF4] and [BMIM][PF6] but slightly underestimate the conductivity for [BMIM][TFSI].

As it was proposed in early studies,[10,11,16,27,40] the conductivity relaxation process corresponds to local ion rearrangements, and from knowledge of the conductivity relaxation time and diffusion coefficient, D, measured by pulsed field gradient nuclear magnetic resonance (PFG-NMR), we can estimate the ion rearrangement length, λ, with

$$\lambda = \sqrt{6D\tau_\sigma} \tag{4}$$

The parameter, λ, defines the characteristic length, where anomalous subdiffusion regime crosses over into a normal Fickian diffusion, and in typical ILs, its value is about $\lambda \approx 1-3$ Å.[27,62] Using the diffusion coefficients of the cation and anion,[23,63] we can estimate separately the rearrangement length for positive and negative charge carriers: $\lambda_+ = \sqrt{6D_+\tau_\sigma}$ and $\lambda_- = \sqrt{6D_-\tau_\sigma}$. These parameters for the studied ILs appear in the range ≈1.2−1.9 Å (Figure.3b). It was suggested[10] that the ion rearrangement length should be about half the average distance between the ions estimated from their concentration, $\langle d \rangle_{conc}/2 = [(3/4\pi n)^{1/3}]/2$. However, the distance estimated from ion concentration appears slightly larger than λ,$\langle d \rangle_{conc}/2 \sim 2.0-2.4$ Å (Figure 3b). The average distance between the ions can also be estimated from the radial distribution function (RDF) obtained from the MD simulations (Figure 3a). Half of the average distance between the ions estimated from the RDF is even slightly larger than $\langle d \rangle_{conc}/2$ (Figure 3b).

Although the estimated rearrangement length, λ, is slightly smaller than the average distance estimated from the ion concentration and RDFs, it is worth noting that its value is almost temperature-independent. This fact can be used for an estimation of the ion diffusion coefficient at low temperatures where slow ion dynamics is inaccessible from PFG-NMR measurements. Indeed, knowing the value of the parameter λ, we can invert eq 4 and use τ_σ from the BDS measurements to estimate the diffusivity of the ions even at low temperatures $D_\pm = \lambda_\pm^2/6\tau_\sigma$.[10,40] The result of these estimations is presented in Figure 4. In the same figure, we presented diffusion coefficients

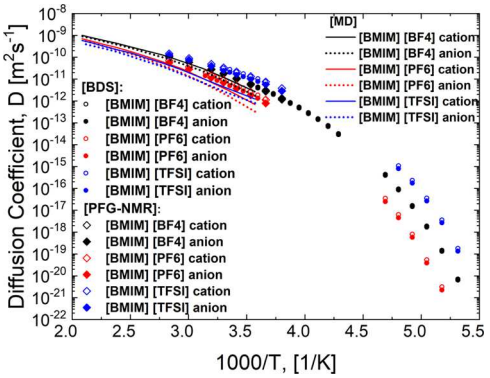

Figure 4. Temperature dependence of the diffusion coefficient for cations and anions of the ILs. Circle symbols represent our experimental data, which are in good agreement with previous studies (ref 23). PFG-NMR data are shown with diamond symbols, and the MD simulation results are shown as solid and dotted lines for the cations and anions, respectively.

from MD simulation, which has a good match with PFG-NMR data for [BMIM][BF4] and [BMIM][PF6] but slightly underestimates diffusion for [BMIM][TFSI]. This is consistent with an underestimated conductivity for the same IL (Figure 2a).

From the diffusion coefficient, we can estimate the expected NE ionic conductivity using eq 1 and calculate the inverse Haven ratio, $H^{-1} = \sigma_{DC}/\sigma_{NE}$, (eq 2) to reveal how ion−ion correlations depend on temperature. Analysis of the inverse Haven ratio in the studied systems (Figure 5) reveals that it remains almost constant ~0.6−0.8 at higher temperatures and

https://doi.org/10.1021/acs.jpcb.3c05568
J. Phys. Chem. B 2023, 127, 10411−10421

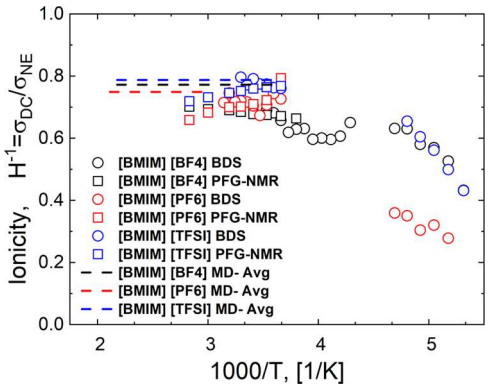

Figure 5. Temperature dependence of the ionicity or the inverse Haven ratio. Circle symbols represent our experimental data, where the diffusion coefficient was estimated from the ac−dc crossover and square symbols corresponds to data, where the diffusion coefficient was measured by PFG-NMR results. The dashed lines represent the average value of ionicity from the MD simulations, which are in good agreement with the experimental data. The complete data obtained from the MD simulations, along with computed standard deviations, are reported in Figure S1b.

then decreases to ∼0.4−0.25 upon cooling toward T_g. The decrease of H^{-1} upon cooling has been reported for many other systems,[10,27] and the mechanism behind this behavior remains unknown.

Although the inverse Haven ratio provides information about ion correlations, this parameter does not reveal any mechanistic details that dominate these correlations in the studied systems. At the same time, the direct experimental measurement of distinct ion−ion correlations is quite difficult.[37] However, the contributions of distinct ion−ion correlations to conductivity can be estimated based on the model proposed by Schonert and developed in several papers.[28,38,39] The model only assumes that the total momentum of all ions is conserved and that the velocities of the cations and anions obey the following equation (the validity of this assumption will be discussed later):

$$M_+ \sum_i \vec{v}_{i+}(0) + M_- \sum_i \vec{v}_{i-}(0) = 0 \tag{5}$$

Considering the case when all ions are mobile, we can multiply eq 5 by $\vec{v}_{j+}(t)$ and $\vec{v}_{j-}(t)$ and take the average to obtain the following pair of equations:

$$\begin{cases} M_+(D^s_+ + D^d_{++}/2) = -M_- D^d_{+-}/2 \\ M_-(D^s_- + D^d_{--}/2) = -M_+ D^d_{+-}/2 \end{cases} \tag{6}$$

where D^s_+ and D^s_- are self-diffusion coefficients and D^d_{++}, D^d_{--}, and D^d_{+-} are distinct diffusion coefficients defined by the relationships

$$\begin{aligned} D^s_+ &= \frac{1}{3}\int_0^\infty \langle \vec{v}_{i+}(t)\vec{v}_{i+}(0)\rangle \mathrm{d}t, \\ D^s_- &= \frac{1}{3}\int_0^\infty \langle \vec{v}_{i-}(t)\vec{v}_{i-}(0)\rangle \mathrm{d}t \\ D^d_{++} &= \frac{\varphi}{3}\int_0^\infty \langle \vec{v}_{i+}(t)\vec{v}_{j+}(0)\rangle \mathrm{d}t, \\ D^d_{--} &= \frac{\varphi}{3}\int_0^\infty \langle \vec{v}_{i-}(t)\vec{v}_{j-}(0)\rangle \mathrm{d}t \\ D^d_{+-} &= \frac{\varphi}{3}\int_0^\infty \langle \vec{v}_{i+}(t)\vec{v}_{j-}(0)\rangle \mathrm{d}t = \frac{\varphi}{3}\int_0^\infty \langle \vec{v}_{i-}(t)\vec{v}_{j+}(0)\rangle \mathrm{d}t \end{aligned} \tag{7}$$

Here, the −/+ subscript refers to either anion/cation, φ is the total number of correlated ions in a local area, and $i \neq j$. Using the definition of conductivity as a current−current correlation function[9,20,21]

$$\begin{aligned} \sigma_{DC} &= \frac{1}{3Vk_BT}\int_0^\infty \langle \vec{J}(0)\cdot\vec{J}(t)\rangle \mathrm{d}t, \text{ with } \langle \vec{J}(0)\cdot\vec{J}(t)\rangle \\ &= \langle \sum_i q_i\vec{v}_i(0)\cdot \sum_j q_j\vec{v}_j(t)\rangle \end{aligned} \tag{8}$$

we have, together with eqs 6 and 8, the closed system of equations for D^d_{++}, D^d_{--}, and D^d_{+-}. To find the contribution of distinct ion−ion correlations into conductivity we can write conductivity as[28,38,39]

$$\sigma_{DC} = \sigma_{NE} + \sigma^d_{+-} + \sigma^d_{++} + \sigma^d_{--}, \quad \sigma_{NE} = \sigma^s_+ + \sigma^s_- \tag{9}$$

where we combined self-correlation to NE conductivity eq 1, and the last three terms define conductivity contribution from distinct anion−cation (σ^d_{+-}), cation−cation (σ^d_{++}), and anion−anion (σ^d_{--}) correlations. As a result, after solving[28,38−40] system of eqs 6 and 8, we can derive analytical expressions for the contribution of the ion−ion correlation in each term of eq 9

$$\begin{aligned} \sigma^d_{++} &= \frac{1}{2}\frac{e^2n}{k_BT}D^d_{++} = \sigma_{DC}\left(\frac{M_-}{M_- + M_+}\right)^2 - \sigma^s_+, \\ \sigma^s_+ &= \frac{e^2n}{k_BT}D^s_+ \\ \sigma^d_{--} &= \frac{1}{2}\frac{e^2n}{k_BT}D^d_{--} = \sigma_{DC}\left(\frac{M_+}{M_- + M_+}\right)^2 - \sigma^s_-, \\ \sigma^s_- &= \frac{e^2n}{k_BT}D^s_- \\ \sigma^d_{+-} &= -\frac{e^2n}{k_BT}D^d_{+-} = \sigma_{DC}\frac{2M_+M_-}{(M_- + M_+)^2} \end{aligned} \tag{10}$$

This result provides a simple means to estimate distinct ion−ion correlations if the DC conductivity and self-diffusion coefficients are experimentally measured. According to eq 10, the cation−anion correlations in ionic liquids always have a positive contribution to conductivity, unlike the systems with a solvent, where this type of correlation might change sign, depending on the solvent concentration.[40] This indicates that the conductivity of the ionic liquids is always improved by the correlated anion−cation motion. The distinct contributions to conductivity estimated by eq 10 and scaled by the expected NE conductivity for the three IL systems studied here are shown in Figure 6. These contributions appear in surprisingly good

https://doi.org/10.1021/acs.jpcb.3c05568
J. Phys. Chem. B 2023, 127, 10411−10421

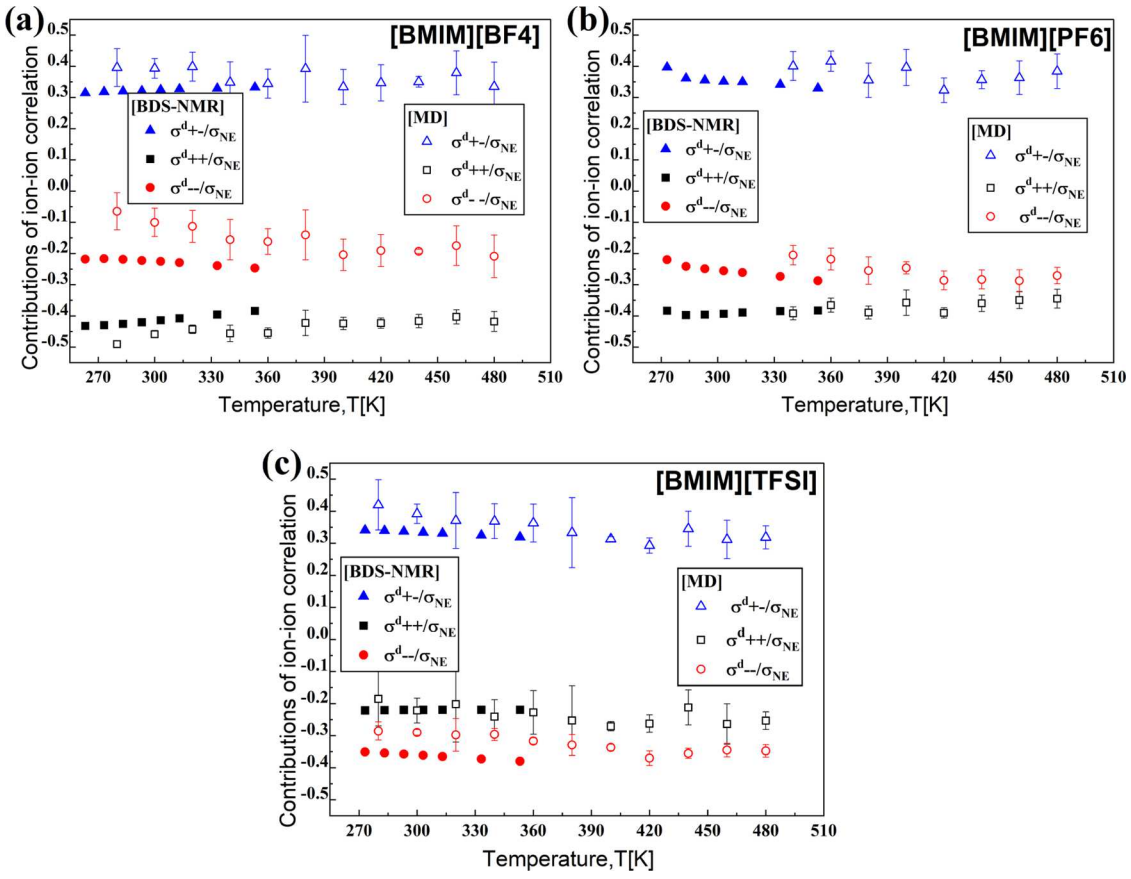

Figure 6. Distinct ion−ion contribution to conductivity normalized by σ_{NE} for the three ILs, where the closed symbols represent our experimental data and open symbols represent data from our MD simulations.

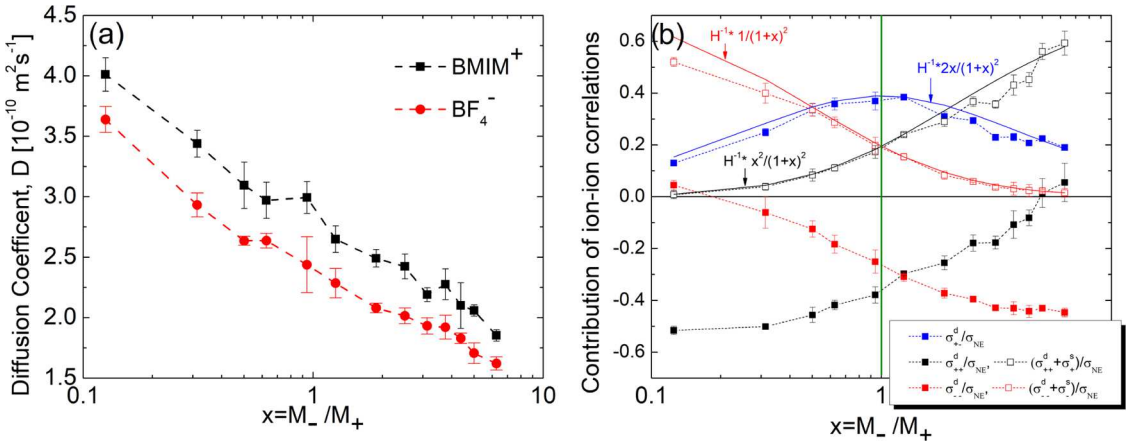

Figure 7. (a) Self-diffusion coefficient as a function of the anion-to-cation mass ratio, $x = M_-/M_+$, at 400 K obtained by MD simulations. (b) Contributions of distinct (closed symbols) and total (open symbols) ion−ion correlations to conductivity normalized by σ_{NE} of [BMIM][BF4] ionic liquids as a function of the artificially changed anion-to-cation mass ratio, $x = M_-/M_+$, at 400 K. The green vertical line indicates the case in which the masses of anion and cation are equal. The solid lines present the theoretical prediction from eq 10, where we used $H^{-1} = 0.78$.

agreement with the direct calculations of these correlations from our MD simulations (Figures 6 and S2). These important results suggest that momentum conservation likely plays an important role in ionic correlations in liquid electrolytes.

Both experimental and simulation results also revealed a significant role of the anion mass in these correlations (Figure 6). While the contribution of the anion−cation correlations to conductivity remains essentially the same, ∼+(0.3−0.4), distinct anion−anion correlations decrease from ∼−0.2 in the IL with (the light) BF_4 to ∼−(0.4−0.5) in the IL with the heavier TFSI, and distinct cation−cation correlations have opposite behavior with the increase of anion mass (Figure 6). Moreover, it can be seen from eq 10 that the mass of the ions has a direct relationship with the distinct ion−ion correlations. In BMIM-BF_4, the mass of the cation is larger than the mass of the anion, resulting in stronger negative cation−cation contributions to the conductivity (Figure 6a), but BMIM-TFSI, where the anion mass is larger than the cation mass, has

https://doi.org/10.1021/acs.jpcb.3c05568
J. Phys. Chem. B 2023, 127, 10411−10421

stronger negative anion−anion contributions to conductivity (Figure 6c). The independent MD simulations reveal a similar result of switching anion−anion and cation−cation correlations with the change of the anion mass (Figure 6). Surprisingly, in [BMIM][PF6], where the anion and cation have similar masses, the cation−cation correlations appear more negative (stronger). The same result is observed in the MD simulations (Figure 6b). This surprising result might be related to the difference in the size/geometry/structure of these ions and their diffusion. Indeed, it was shown[64] that in the case of [EMIM][TFSI], cation and anion diffusion coefficients have different dependence on the applied pressure, corresponding to the connection between TFSI conformational exchange and diffusion. It appears[23] that the diffusion of BMIM cation is faster than the diffusion of any studied here anions, regardless of their mass. The good agreement between the estimates of the distinct ionic correlations from the experimental data using eq 10 and the results of the MD simulations justifies a simple approach based on momentum conservation for the analysis of distinct ion−ion correlations in the various ionic systems.

To better understand the impact of the mass of the anion, we artificially manipulated the mass of BF_4^- in the MD simulations across a broad spectrum of molecular weight while maintaining the same force field. This approach enabled us to eliminate the influence of other factors, including the anion structure and charge distribution. As expected, the self-diffusion coefficient of the anion decreases with increasing mass. Similar behavior is observed for the cation (Figure 7a). It is worth noting that the self-diffusivity of the cation is consistently greater than that of the anion across all of the studied cases ($M_-/M_+ = 0.125 - 6.26$). This occurrence can be explained by the geometry of the cation, which leads to a preferential translational motion in the plane of the ring.[48,65] Spatial distribution functions (SDFs) of these ILs show that the anions preferentially present above/below the imidazolium ring generally close to the top carbon, while the area near the nonpolar alkyl tails remains vacant (Figure 8 top), leading to a preferential direction for the movement of the cation. In addition, the surfaces become larger with decreasing size of the anion. This characteristic has been observed previously in both experimental and computational studies.[24,65−72] In contrast, the SDFs of the BMIM cation around the three anions reveal that the BMIM cation distributes around the anions in a symmetric and well-ordered way, especially noticeable for the PF6 and BF4 anions (forming an octahedron for PF6 and a tetrahedron for BF4, respectively), as depicted in the bottom panel of Figure 8. It is worth noting that the BMIM cation resides around the linear TFSI anion, contributing to the fast movement of the anion in BMIM-TFSI system, despite TFSI being heavier than the other two anions. However, this specific phenomenon was not captured in our simulations due to the limitations in the force field, which could not adequately represent the multiple conformations of the TFSI anion.[73] Not surprisingly, changes in the anion mass have a negligible influence on the distribution of cations around the anion and the anions around the cation, as shown in Figure S3. This phenomenon elucidates why the [BMIM] cation exhibits diffusion faster than that of the anion across a wide range of anion-to-cation mass ratios (Figure 7a). The relaxation time of ion-association increases with an increase in the mass of the anion (Figure S4). This implies that heavier ions require more time to escape the cage formed by oppositely charged ions. In addition, our MD simulations reveal the heterogeneity of the nonpolar domains. The anion exhibits a minimal influence on the clustering of these nonpolar domains, which is represented by the tail groups of the imidazolium ring (Figure S5). However, previous reports indicate that increasing the tail length significantly increases the aggregation of nonpolar domains in coarse-grained modeling of $[C_xMIM][NO_3]$ (x = 1, 2, 3, 4, 6, and 8) systems.[74]

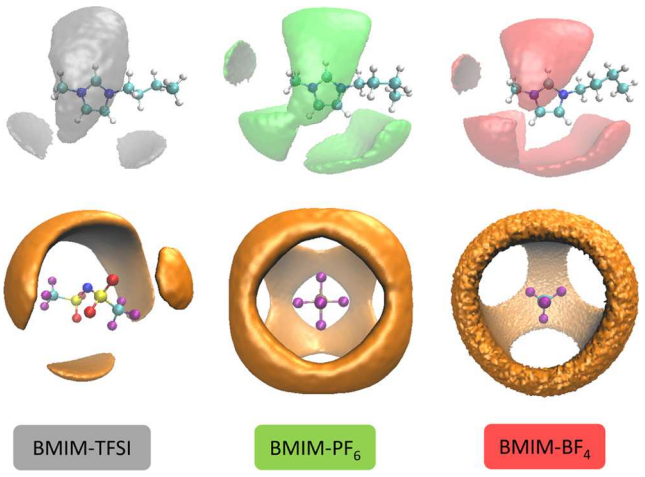

Figure 8. Spatial distribution functions of anions around the BMIM cation (top) and the BMIM cation around three anions (bottom). The SDFs were computed using the TRAVIS program[75] and visualized by the VMD program.[76] The contour surfaces are shown at the isovalues of 10 nm^{-3} and 6 nm^{-3} for the top and bottom ones, respectively.

The contribution of distinct ion−ion correlations normalized by σ_{NE} as a function of the anion-to-cation mass ratio were also examined (Figure 7b). We found that the correlated movement of the cations and anions positively contributes to the conductivity, while the distinct correlations between ions of the same charge result in negative contributions to the conductivity. More specifically, the negative contribution of distinct anion−anion correlation increases with an increase in the mass of the anion. In contrast, the distinct cation−cation correlation shows an opposite trend. Moreover, all of the distinct correlations quickly change when the anion-to-cation mass ratio is very small or very large. This is consistent with the difference between the distinct like-charged ion correlations in the case of an anion lighter than the cation (Figure 6a) and the opposite situation (Figure 6c). It is worth noting that the distinct anion−anion correlation coincides with the distinct cation−cation correlation when the ratio of the anion-to-cation mass (M_-/M_+) equals 1.25, rather than when the masses are identical, as indicated by the green vertical line in Figure 7b. This shift is consistent with stronger negative σ^d_{++} than σ^d_{--} in the [BMIM][PF6] system with $M_+ \sim M_-$ (Figure 6b). The shift of the crossing between the distinct ion correlations is related to the differences in diffusion coefficients of anion and cation, which may be due to the anisotropic diffusion of the cation compared to the isotropic movement of the anion, as discussed above. Indeed, if we take into account the self-correlations, we obtain that $\Delta^{total}_- = (\sigma^d_{--} + \sigma^s_-)/\sigma_{NE}$ and $(\Delta^d_- + \sigma^s_-)/\sigma_{NE}$ switch exactly at $M_- = M_+$ (Figure 7b), in agreement with eq 10. Furthermore, eq 10 correctly predicts how normalized cation−anion correlations $\sigma^d_{+-}/\sigma_{NE}$ and total contribution Δ^{total}_+ and Δ^{total}_- depend on mass (solid lines in

https://doi.org/10.1021/acs.jpcb.3c05568
J. Phys. Chem. B 2023, 127, 10411−10421

Figure 7b). Surprisingly, the distinct like-charged ion correlations shift from negative to slightly positive values, as the ratio of anion-to-cation masses is either significantly small or sufficiently large. The reason for this remains unclear. These findings conclusively demonstrate that disparities in the anion and cation masses influence the magnitude of distinct correlations between ions. Remarkably, even the sign of these contributions can change when the masses of the ions are significantly different. However, the results (Figures 6 and 7b) also suggest that the ion mass is not the only parameter affecting these correlations. Apparently, the geometry and/or volume of the ions and their diffusion also play a role.

It is important to emphasize that the MD simulations explicitly assume momentum conservation (keeping no displacement for the center of mass). The law of momentum conservation in the form of eq 5 assumes that total momentum is conserved only for mobile ions and is not transferred to the environment, e.g., to the sample cell. It is equivalent when the coordinate system is linked to the center of mass, where the velocity of the center of mass of the system is zero, i.e.,

$$\vec{v}_{CM}(t) = \frac{M_+\vec{v}_+(t) + M_-\vec{v}_-(t)}{M_+ + M_-} = 0 \quad (11)$$

However, recent studies using electrophoretic NMR[77] suggest that momentum conservation might be broken in ILs, and instead, the conservation of local molar volumes of specific ions may play a critical role. In this case, the velocity of the center of mass of the system might not be equal to zero $\vec{v}_{CM}(t) \neq 0$, and we have to take into account the next type of correlations $\langle \vec{v}_{CM}(t)\vec{v}_{CM}(0)\rangle$, $\langle \vec{v}_+(t)\vec{v}_{CM}(0)\rangle$ and $\langle \vec{v}_-(t)\vec{v}_{CM}(0)\rangle$. The general equations in this case have been derived in refs.78,79. The effect of these three additional terms is difficult to estimate because it is quite challenging to measure how much momentum has passed to the environment due to the movement of the ions. One of the ways to measure this is to compare the MD simulations, which explicitly assume momentum conservation only between ions and experimentally measured distinct ion−ion correlations, as proposed in 37.

CONCLUSIONS

In this work, we studied three ILs with different anion/cation mass ratios. We have measured conductivity spectra over a wide frequency range and estimated DC conductivity and conductivity relaxation times over a wide temperature range. Based on the diffusion coefficient at high temperatures, we estimated the ion rearrangement length, marking a crossover from anomalous to normal diffusion regime. This length appears slightly shorter than half of the average distance of the ions assumed in earlier studies. It is important that in the accessible temperature range, this length scale appears essentially temperature-independent. This enables an estimate of ion diffusion at low temperatures, where it is too slow for PFG-NMR. As a result, it provides a way to estimate the inverse Haven ratio at very low temperatures. Our results indicate that H^{-1} decreases with decreasing temperature, but the mechanism of this temperature dependence requires additional investigation. Furthermore, we demonstrate that the distinct ion−ion contributions to conductivity can be estimated using a momentum conservation approach in the center of mass coordinate system. The results from this approach were validated by our MD simulations. It was discovered that the behavior of the anion−anion and cation−cation correlations depend strongly on the anion-to-cation mass ratio, M_-/M_+. In the case of $M_-/M_+ > 1$, the distinct anion−anion correlations show a stronger suppression effect in the conductivity in comparison to the distinct cation−cation correlation. The opposite effect is observed in the case of $M_-/M_+ < 1$. This switching effect was also verified by our MD simulations. A detailed analysis also revealed that not only mass but also the diffusivity of ions plays a role in these correlations, emphasizing the role of ion geometry.

ASSOCIATED CONTENT

Data Availability Statement

The data that support the plots within this paper and another finding of this study are available from the corresponding author upon reasonable request.

Supporting Information

The Supporting Information is available free of charge at https://pubs.acs.org/doi/10.1021/acs.jpcb.3c05568.

Comparison of simulated and experimental densities; simulated inverse Haven ratio; MD simulations of distinct ion−ion contribution to conductivity for all three systems; spatial distribution functions; continuous and intermittent time correlation functions at different mass ratios; snapshots of different groups and radial distribution functions (PDF)

AUTHOR INFORMATION

Corresponding Author

Ivan Popov − *Department of Chemistry, University of Tennessee, Knoxville, Tennessee 37996, United States; University of Tennessee—Oak Ridge Innovation Institute, University of Tennessee, Knoxville, Tennessee 37996, United States;* orcid.org/0000-0002-7235-2043; Email: ipopov@utk.edu

Authors

Md. Dipu Ahmed − *Department of Chemistry, University of Tennessee, Knoxville, Tennessee 37996, United States*

Zhenghao Zhu − *Department of Chemical Engineering, University of Tennessee, Knoxville, Tennessee 37996, United States;* orcid.org/0000-0001-9748-3894

Airat Khamzin − *Institute of Physics, Kazan Federal University, Kazan 420008, Russia;* orcid.org/0000-0001-9741-4346

Stephen J. Paddison − *Department of Chemical Engineering, University of Tennessee, Knoxville, Tennessee 37996, United States;* orcid.org/0000-0003-1064-8233

Alexei P. Sokolov − *Department of Chemistry, University of Tennessee, Knoxville, Tennessee 37996, United States; Chemical Sciences Division, Oak Ridge National Laboratory, Oak Ridge, Tennessee 37831, United States;* orcid.org/0000-0002-8187-9445

Complete contact information is available at: https://pubs.acs.org/10.1021/acs.jpcb.3c05568

Author Contributions

M.D.A. and I.P. performed the dielectric measurements over a wide range of frequencies and analyzed the conductivity data. Z.Z. and S.J.P. performed molecular dynamics simulations. All authors contributed to the discussion of the results and writing of the manuscript.

Notes

The authors declare no competing financial interest.
The computer code used for simulations is available from the corresponding authors upon reasonable request.

■ ACKNOWLEDGMENTS

This work was supported by the National Science Foundation (award CHE-2102425). Computing resources were provided through an ACCESS allocation DMR130078 on Purdue Anvil CPU. A.Kh. is grateful for support by the Kazan Federal University Strategic Academic Leadership Program (Priority-2030).

■ REFERENCES

(1) Watanabe, M.; Thomas, M. L.; Zhang, S.; Ueno, K.; Yasuda, T.; Dokko, K. Application of Ionic Liquids to Energy Storage and Conversion Materials and Devices. *Chem. Rev.* **2017**, *117*, 7190−7239.
(2) Goodenough, J. B.; Park, K.-S. The Li-Ion Rechargeable Battery: A Perspective. *J. Am. Chem. Soc.* **2013**, *135*, 1167−1176.
(3) Suo, L.; Hu, Y.-S.; Li, H.; Armand, M.; Chen, L. A new class of solvent-in-salt electrolyte for high-energy rechargeable metallic lithium batteries. *Nat. Commun.* **2013**, *4*, No. 1481, DOI: 10.1038/ncomms2513.
(4) Zeng, X.; Li, J. Innovative application of ionic liquid to separate Al and cathode materials from spent high-power lithium-ion batteries. *J. Hazard. Mater.* **2014**, *271*, 50−56.
(5) Shah, F. U.; An, R.; Muhammad, N. Editorial: Properties and Applications of Ionic Liquids in Energy and Environmental Science. *Front. Chem.* **2020**, *8*, No. 627213.
(6) Yoo, K. S. Synthesis of TiO2 Materials Using Ionic Liquids and Its Applications for Sustainable Energy and Environment. *J. Nanosci. Nanotechnol.* **2016**, *16*, 4302−4309.
(7) Sippel, P.; Lunkenheimer, P.; Krohns, S.; Thoms, E.; Loidl, A. Importance of liquid fragility for energy applications of ionic liquids. *Sci. Rep.* **2015**, *5*, No. 13922.
(8) Rauber, D.; Hofmann, A.; Philippi, F.; Kay, C. W. M.; Zinkevich, T.; Hanemann, T.; Hempelmann, R. Structure-Property Relation of Trimethyl Ammonium Ionic Liquids for Battery Applications. *Appl. Sci.* **2021**, *11*, No. 5679, DOI: 10.3390/app11125679.
(9) Maass, P.; Meyer, M.; Bunde, A. Nonstandard relaxation behavior in ionically conducting materials. *Phys. Rev. B* **1995**, *51*, 8164−8177.
(10) Gainaru, C.; Stacy, E. W.; Bocharova, V.; Gobet, M.; Holt, A. P.; Saito, T.; Greenbaum, S.; Sokolov, A. P. Mechanism of Conductivity Relaxation in Liquid and Polymeric Electrolytes: Direct Link between Conductivity and Diffusivity. *J. Phys. Chem. B* **2016**, *120*, 11074−11083.
(11) Stacy, E. W.; Gainaru, C. P.; Gobet, M.; Wojnarowska, Z.; Bocharova, V.; Greenbaum, S. G.; Sokolov, A. P. Fundamental Limitations of Ionic Conductivity in Polymerized Ionic Liquids. *Macromolecules* **2018**, *51*, 8637−8645.
(12) Vargas-Barbosa, N. M.; Roling, B. Dynamic Ion Correlations in Solid and Liquid Electrolytes: How Do They Affect Charge and Mass Transport? *ChemElectroChem* **2020**, *7*, 367−385.
(13) MacFarlane, D. R.; Forsyth, M.; Izgorodina, E. I.; Abbott, A. P.; Annat, G.; Fraser, K. On the concept of ionicity in ionic liquids. *Phys. Chem. Chem. Phys.* **2009**, *11*, 4962−4967.
(14) Murch, G. E. The haven ratio in fast ionic conductors. *Solid State Ionics* **1982**, *7*, 177−198.
(15) Noda, A.; Hayamizu, K.; Watanabe, M. Pulsed-Gradient Spin−Echo 1H and 19F NMR Ionic Diffusion Coefficient, Viscosity, and Ionic Conductivity of Non-Chloroaluminate Room-Temperature Ionic Liquids. *J. Phys. Chem. B* **2001**, *105*, 4603−4610.
(16) Sangoro, J. R.; Kremer, F. Charge Transport and Glassy Dynamics in Ionic Liquids. *Acc. Chem. Res.* **2012**, *45*, 525−532.
(17) Angell, C. A. Diffusion—Conductance Relations and Free Volume in Molten Salts. *J. Phys. Chem. A* **1965**, *69*, 399−403.
(18) Bockris, J. O. M.; Hooper, G. W. Self-diffusion in molten alkali halides. *Discuss. Faraday Soc.* **1961**, *32*, 218−236.
(19) Spedding, P. L.; Mills, R. Trace-Ion Diffusion in Molten Alkali Carbonates. *J. Electrochem. Soc.* **1965**, *112*, No. 594, DOI: 10.1149/1.2423614.
(20) Dyre, J. C.; Maass, P.; Roling, B.; Sidebottom, D. L. Fundamental questions relating to ion conduction in disordered solids. *Rep. Prog. Phys.* **2009**, *72*, No. 046501.
(21) Roling, B.; Martiny, C.; Brückner, S. Ion transport in glass: Influence of glassy structure on spatial extent of nonrandom ion hopping. *Phys. Rev. B* **2001**, *63*, No. 214203.
(22) Zhang, Z.; Wheatle, B. K.; Krajniak, J.; Keith, J. R.; Ganesan, V. Ion Mobilities, Transference Numbers, and Inverse Haven Ratios of Polymeric Ionic Liquids. *ACS Macro Lett.* **2020**, *9*, 84−89.
(23) Tokuda, H.; Hayamizu, K.; Ishii, K.; Susan, M. A. B. H.; Watanabe, M. Physicochemical Properties and Structures of Room Temperature Ionic Liquids. 1. Variation of Anionic Species. *J. Phys. Chem. B* **2004**, *108*, 16593−16600, DOI: 10.1021/jp047480r.
(24) Tokuda, H.; Hayamizu, K.; Ishii, K.; Susan, M. A. B. H.; Watanabe, M. Physicochemical Properties and Structures of Room Temperature Ionic Liquids. 2. Variation of Alkyl Chain Length in Imidazolium Cation. *J. Phys. Chem. B* **2005**, *109*, 6103−6110, DOI: 10.1021/jp044626d.
(25) Tokuda, H.; Ishii, K.; Susan, M. A. B. H.; Tsuzuki, S.; Hayamizu, K.; Watanabe, M. Physicochemical Properties and Structures of Room-Temperature Ionic Liquids. 3. Variation of Cationic Structures. *J. Phys. Chem. B* **2006**, *110*, 2833−2839, DOI: 10.1021/jp053396f.
(26) Tokuda, H.; Tsuzuki, S.; Susan, M. A. B. H.; Hayamizu, K.; Watanabe, M. How Ionic Are Room-Temperature Ionic Liquids? An Indicator of the Physicochemical Properties. *J. Phys. Chem. B* **2006**, *110*, 19593−19600, DOI: 10.1021/jp064159v.
(27) Sangoro, J. R.; Serghei, A.; Naumov, S.; Galvosas, P.; Kärger, J.; Wespe, C.; Bordusa, F.; Kremer, F. Charge transport and mass transport in imidazolium-based ionic liquids. *Phys. Rev. E* **2008**, *77*, No. 051202.
(28) Kashyap, H. K.; Annapureddy, H. V. R.; Raineri, F. O.; Margulis, C. J. How Is Charge Transport Different in Ionic Liquids and Electrolyte Solutions? *J. Phys. Chem. B* **2011**, *115*, 13212−13221.
(29) Harris, K. R. Relations between the Fractional Stokes−Einstein and Nernst−Einstein Equations and Velocity Correlation Coefficients in Ionic Liquids and Molten Salts. *J. Phys. Chem. B* **2010**, *114*, 9572−9577.
(30) Harris, K. R. Can the Transport Properties of Molten Salts and Ionic Liquids Be Used To Determine Ion Association? *J. Phys. Chem. B* **2016**, *120*, 12135−12147.
(31) Harris, K. R.; Kanakubo, M. Self-Diffusion Coefficients and Related Transport Properties for a Number of Fragile Ionic Liquids. *J. Chem. Eng. Data* **2016**, *61*, 2399−2411.
(32) Brinkkötter, M.; Mariani, A.; Jeong, S.; Passerini, S.; Schönhoff, M. Ionic Liquid in Li Salt Electrolyte: Modifying the Li+ Transport Mechanism by Coordination to an Asymmetric Anion. *Adv. Energy Sustainability Res.* **2021**, *2*, No. 2000078, DOI: 10.1002/aesr.202000078.
(33) McEldrew, M.; Goodwin, Z. A. H.; Molinari, N.; Kozinsky, B.; Kornyshev, A. A.; Bazant, M. Z. Salt-in-Ionic-Liquid Electrolytes: Ion Network Formation and Negative Effective Charges of Alkali Metal Cations. *J. Phys. Chem. B* **2021**, *125*, 13752−13766.
(34) Molinari, N.; Mailoa, J. P.; Craig, N.; Christensen, J.; Kozinsky, B. Transport anomalies emerging from strong correlation in ionic liquid electrolytes. *J. Power Sources* **2019**, *428*, 27−36.
(35) Molinari, N.; Mailoa, J. P.; Kozinsky, B. General Trend of a Negative Li Effective Charge in Ionic Liquid Electrolytes. *J. Phys. Chem. Lett.* **2019**, *10*, 2313−2319.
(36) Nürnberg, P.; Atik, J.; Borodin, O.; Winter, M.; Paillard, E.; Schönhoff, M. Superionicity in Ionic-Liquid-Based Electrolytes

Induced by Positive Ion−Ion Correlations. *J. Am. Chem. Soc.* **2022**, *144*, 4657−4666.
(37) Dong, D.; Sälzer, F.; Roling, B.; Bedrov, D. How efficient is Li+ ion transport in solvate ionic liquids under anion-blocking conditions in a battery? *Phys. Chem. Chem. Phys.* **2018**, *20*, 29174−29183.
(38) Schoenert, H. J. Evaluation of velocity correlation coefficients from experimental transport data in electrolytic systems. *J. Phys. Chem. A* **1984**, *88*, 3359−3363.
(39) Popov, I.; Biernacka, K.; Zhu, H.; Nti, F.; Porcarelli, L.; Wang, X.; Khamzin, A.; Gainaru, C.; Forsyth, M.; Sokolov, A. P. Strongly Correlated Ion Dynamics in Plastic Ionic Crystals and Polymerized Ionic Liquids. *J. Phys. Chem. C* **2020**, *124*, 17889−17896.
(40) Popov, I.; Khamzin, A.; Matsumoto, R. A.; Zhao, W.; Lin, X.; Cummings, P. T.; Sokolov, A. P. Controlling the Ion Transport Number in Solvent-in-Salt Solutions. *J. Phys. Chem. B* **2022**, *126*, 4572−4583.
(41) Ishai, P. B.; Talary, M. S.; Caduff, A.; Levy, E.; Feldman, Y. Electrode polarization in dielectric measurements: a review. *Meas. Sci. Technol.* **2013**, *24*, No. 102001.
(42) Liu, H.; Luo, X.; Sokolov, A. P.; Paddison, S. J. Quantitative Evidence of Mobile Ion Hopping in Polymerized Ionic Liquids. *J. Phys. Chem. B* **2021**, *125*, 372−381.
(43) Luo, X.; Liu, H.; Paddison, S. J. Molecular Dynamics Simulations of Polymerized Ionic Liquids: Mechanism of Ion Transport with Different Anions. *ACS Appl. Polym. Mater.* **2021**, *3*, 141−152.
(44) Mogurampelly, S.; Keith, J. R.; Ganesan, V. Mechanisms Underlying Ion Transport in Polymerized Ionic Liquids. *J. Am. Chem. Soc.* **2017**, *139*, 9511−9514.
(45) Sprenger, K. G.; Jaeger, V. W.; Pfaendtner, J. The General AMBER Force Field (GAFF) Can Accurately Predict Thermodynamic and Transport Properties of Many Ionic Liquids. *J. Phys. Chem. B* **2015**, *119*, 5882−5895.
(46) Slingsby, J. G.; Vyas, S.; Maupin, C. M. A charge-modified general amber force field for phospholipids: improved structural properties in the tensionless ensemble. *Mol. Simul.* **2015**, *41*, 1449−1458.
(47) Liu, H.; Maginn, E.; Visser, A. E.; Bridges, N. J.; Fox, E. B. Thermal and transport properties of six ionic liquids: An experimental and molecular dynamics study. *Ind. Eng. Chem. Res.* **2012**, *51*, 7242−7254.
(48) Liu, H.; Maginn, E. A molecular dynamics investigation of the structural and dynamic properties of the ionic liquid 1-n-butyl-3-methylimidazolium bis(trifluoromethanesulfonyl) imide. *J. Chem. Phys.* **2011**, *135*, No. 124507.
(49) Bayly, C. I.; Cieplak, P.; Cornell, W.; Kollman, P. A. A well-behaved electrostatic potential based method using charge restraints for deriving atomic charges: the RESP model. *J. Phys. Chem. A* **1993**, *97*, 10269−10280.
(50) Frisch, M. J.; Trucks, G. W.; Schlegel, H. B.; Scuseria, G. E.; Robb, M. A.; Cheeseman, J. R.; Scalmani, G.; Barone, V.; Mennucci, B.; Petersson, G. A.et al. *Gaussian 09*, Revision E.01; Gaussian, Inc.: Wallingford, CT, 2013.
(51) Zhang, Z.; Zofchak, E.; Krajniak, J.; Ganesan, V. Influence of Polarizability on the Structure, Dynamic Characteristics, and Ion-Transport Mechanisms in Polymeric Ionic Liquids. *J. Phys. Chem. B* **2022**, *126*, 2583−2592.
(52) Barbosa, G. D.; Liu, X.; O'Harra, K. E.; Bara, J. E.; Turner, C. H. Charge scaling parameter evaluation for multivalent ionic liquids with fixed point charge force fields. *J. Ionic Liq.* **2022**, *2*, No. 100020.
(53) Abraham, M. J.; Murtola, T.; Schulz, R.; Páll, S.; Smith, J. C.; Hess, B.; Lindahl, E. GROMACS: High performance molecular simulations through multi-level parallelism from laptops to supercomputers. *SoftwareX* **2015**, *1−2*, 19−25.
(54) Fong, K. D.; Self, J.; McCloskey, B. D.; Persson, K. A. Ion Correlations and Their Impact on Transport in Polymer-Based Electrolytes. *Macromolecules* **2021**, *54*, 2575−2591.
(55) Bussi, G.; Donadio, D.; Parrinello, M. Canonical sampling through velocity rescaling. *J. Chem. Phys.* **2007**, *126*, No. 014101.
(56) Parrinello, M.; Rahman, A. Crystal Structure and Pair Potentials: A Molecular-Dynamics Study. *Phys. Rev. Lett.* **1980**, *45*, 1196−1199.
(57) Dyre, J. C. The random free-energy barrier model for ac conduction in disordered solids. *J. Appl. Phys.* **1988**, *64*, 2456−2468.
(58) Dyre, J. C. Studies of ac hopping conduction at low temperatures. *Phys. Rev. B* **1994**, *49*, 11709−11720.
(59) Dyre, J. C.; Schrøder, T. B. Universality of ac conduction in disordered solids. *Rev. Mod. Phys.* **2000**, *72*, 873−892.
(60) Schrøder, T. B.; Dyre, J. C. Scaling and Universality of ac Conduction in Disordered Solids. *Phys. Rev. Lett.* **2000**, *84*, 310−313.
(61) Schrøder, T. B.; Dyre, J. C. ac Hopping Conduction at Extreme Disorder Takes Place on the Percolating Cluster. *Phys. Rev. Lett.* **2008**, *101*, No. 025901.
(62) Sangoro, J. R.; Iacob, C.; Naumov, S.; Valiullin, R.; Rexhausen, H.; Hunger, J.; Buchner, R.; Strehmel, V.; Kärger, J.; Kremer, F. Diffusion in ionic liquids: the interplay between molecular structure and dynamics. *Soft Matter* **2011**, *7*, 1678−1681.
(63) Popov, I.; Sacci, R. L.; Sanders, N. C.; Matsumoto, R. A.; Thompson, M. W.; Osti, N. C.; Kobayashi, T.; Tyagi, M.; Mamontov, E.; Pruski, M.; et al. Critical Role of Anion−Solvent Interactions for Dynamics of Solvent-in-Salt Solutions. *J. Phys. Chem. C* **2020**, *124*, 8457−8466.
(64) Suarez, S. N.; Rúa, A.; Cuffari, D.; Pilar, K.; Hatcher, J. L.; Ramati, S.; Wishart, J. F. Do TFSA Anions Slither? Pressure Exposes the Role of TFSA Conformational Exchange in Self-Diffusion. *J. Phys. Chem. B* **2015**, *119*, 14756−14765.
(65) Urahata, S. M.; Ribeiro, M. C. C. Single particle dynamics in ionic liquids of 1-alkyl-3-methylimidazolium cations. *J. Chem. Phys.* **2004**, *122*, No. 024511, DOI: 10.1063/1.1826035.
(66) Sarangi, S. S.; Zhao, W.; Müller-Plathe, F.; Balasubramanian, S. Correlation between Dynamic Heterogeneity and Local Structure in a Room-Temperature Ionic Liquid: A Molecular Dynamics Study of [bmim][PF6]. *ChemPhysChem* **2010**, *11*, 2001−2010.
(67) Kanakubo, M.; Harris, K. R.; Tsuchihashi, N.; Ibuki, K.; Ueno, M. Effect of Pressure on Transport Properties of the Ionic Liquid 1-Butyl-3-methylimidazolium Hexafluorophosphate. *J. Phys. Chem. B* **2007**, *111*, 2062−2069.
(68) Bhargava, B. L.; Balasubramanian, S. Refined potential model for atomistic simulations of ionic liquid [bmim][PF6]. *J. Chem. Phys.* **2007**, *127*, No. 114510.
(69) Rey-Castro, C.; Vega, L. F. Transport Properties of the Ionic Liquid 1-Ethyl-3-Methylimidazolium Chloride from Equilibrium Molecular Dynamics Simulation. The Effect of Temperature. *J. Phys. Chem. B* **2006**, *110*, 14426−14435.
(70) Cadena, C.; Zhao, Q.; Snurr, R. Q.; Maginn, E. J. Molecular Modeling and Experimental Studies of the Thermodynamic and Transport Properties of Pyridinium-Based Ionic Liquids. *J. Phys. Chem. B* **2006**, *110*, 2821−2832.
(71) Liu, Z.; Huang, S.; Wang, W. A Refined Force Field for Molecular Simulation of Imidazolium-Based Ionic Liquids. *J. Phys. Chem. B* **2004**, *108*, 12978−12989.
(72) Morrow, T. I.; Maginn, E. J. Molecular Dynamics Study of the Ionic Liquid 1-n-Butyl-3-methylimidazolium Hexafluorophosphate. *J. Phys. Chem. B* **2002**, *106*, 12807−12813.
(73) Fujii, K.; Fujimori, T.; Takamuku, T.; Kanzaki, R.; Umebayashi, Y.; Ishiguro, S.-I. Conformational Equilibrium of Bis-(trifluoromethanesulfonyl) Imide Anion of a Room-Temperature Ionic Liquid: Raman Spectroscopic Study and DFT Calculations. *J. Phys. Chem. B* **2006**, *110*, 8179−8183.
(74) Wang, Y.; Voth, G. A. Unique Spatial Heterogeneity in Ionic Liquids. *J. Am. Chem. Soc.* **2005**, *127*, 12192−12193.
(75) Brehm, M.; Thomas, M.; Gehrke, S.; Kirchner, B. TRAVIS—A free analyzer for trajectories from molecular simulation. *J. Chem. Phys.* **2020**, *152*, No. 164105, DOI: 10.1063/5.0005078.
(76) Humphrey, W.; Dalke, A.; Schulten, K. VMD: Visual molecular dynamics. *J. Mol. Graphics* **1996**, *14*, 33−38.
(77) Lorenz, M.; Kilchert, F.; Nurnberg, P.; Schammer, M.; Latz, A.; Horstmann, B.; Schonhoff, M. Local Volume Conservation in

Concentrated Electrolytes Is Governing Charge Transport in Electric Fields. *J. Phys. Chem. Lett.* **2022**, *13*, 8761−8767.
(78) Pfeifer, S.; Ackermann, F.; Salzer, F.; Schonhoff, M.; Roling, B. Quantification of cation-cation, anion-anion and cation-anion correlations in Li salt/glyme mixtures by combining very-low-frequency impedance spectroscopy with diffusion and electrophoretic NMR. *Phys. Chem. Chem. Phys.* **2021**, *23*, 628−640.
(79) Roling, B.; Miß, V.; Kettner, J. J. E.; Materials, E. Ion Dynamics in Concentrated Electrolyte Solutions: Relating Equilibrium Fluctuations of the Ions to Transport Properties in Battery Cells. *Energy Environ. Mater.* **2022**, No. e12533, DOI: 10.1002/eem2.12533.

https://doi.org/10.1021/acs.jpcb.3c05568
J. Phys. Chem. B 2023, 127, 10411−10421